*Rev. Roum. Sci. Techn.– Électrotechn. et Énerg.*
Vol. **71**, *4*, pp. 531–536, Bucarest, 2026

# ANALYSIS OF A NON-ISOLATED FORM OF DC-DC CONVERTER WITH ENHANCED QUADRATIC VOLTAGE GAIN

MURALI DURAISAMY[1], VIDHARSHAN MURALI[2]

**Keywords: Continuous inductor current; DC-DC power electronic converter; Duty ratio; Prototype converter setup; Quadratic-based voltage gain; Reduced switch voltage stress; Steady-state behavior.**

**Among the various renewable energy resources, the solar photovoltaic (PV) method of electrical energy generation offers advantages such as reduced environmental pollution compared to the conventional fossil fuel method, its availability, and the limitless availability of solar energy. The solar PV panels produce power only at a low DC output voltage. The solar PV array connected to a low-voltage DC bus cannot supply power directly to the high-voltage DC loads. An intermediate high-gain DC-DC power electronic converter is required to enhance the solar PV panel's output voltage. Traditional non-isolated DC-DC boost converter structures can achieve higher DC output voltages only at high duty ratios. A non-isolated continuous inductor current-mode-based DC-DC converter that can produce quadratic-based enhanced voltage gain at low duty cycle is proposed in this paper. The suggested topology has fewer semiconductor-based and passive components and reduces active power-switch voltage stress. The steady-state behavior of the converter is explored. A prototype converter model is constructed and tested in a laboratory environment to validate its results at a duty ratio of 0.6.**

## 1. INTRODUCTION

Recently, the non-isolated and isolated forms of DC-DC power electronic converters with high voltage gain capability play a vital role in renewable energy-based power generation scenarios [1–10]. Medium-power applications employ non-isolated converter structures, whereas high-power applications require isolated converter configurations. There are certain merits and demerits associated with each of the above two topologies. The researchers have developed certain high-voltage gain capability topologies of DC-DC converters using switched inductors (SL), switched capacitors (SC), and voltage multiplier cells (VMC). The DC-DC converters with a combination of switched capacitors and VMCs can be used to achieve higher output voltages. However, this combination causes increased power losses due to the higher amount of charging current [11–13]. The coupled-inductor-based converter topologies can produce high voltage gain by suitable adjustment of their turns ratio. However, this results in a higher percentage of ripples in the input current [14]. The interleaved boost converters with a larger number of VMCs at the output can yield higher DC output voltages at a lower duty factor itself [15].

A transformerless boost-modified Cuk combined structure of a high-gain DC-DC converter is proposed by the author in [16], where the behavior of the converter during the steady state and its mathematical modeling are explored. An integrated single-switch transformerless converter structure consisting of conventional boost and Cuk configurations with reduced passive components capable of providing improved voltage gain is proposed by some authors [17]. Another integrated single-switch transformerless high-gain converter structure comprising the conventional SEPIC and Cuk topologies was proposed in [18], where the converter's dynamic performance is improved using a fractional-order PID (FOPID) controller. The non-isolated single-switch Zeta-Mahafzah converter topologies are suggested by some authors in [19]. The features of the topologies presented in [19] include enhanced reliability and steady-state performance, reduced potential stress across the semiconductor-based components, enhanced high step-up voltage gain at a lower value of duty factor, and the capability of producing multiple DC output voltages that are synchronized. A hybrid coupled-inductor-based single-switch converter structure comprising Luo and flyback topologies with a voltage-boosting module, suitable for application in power generation using renewable sources of energy, is proposed in [20]. The topology presented in [20] has relative merits such as reduced switch voltage stress, improved step-up voltage conversion ratio, lower ripple content in the source current, and high power conversion efficiency due to reduced switching and conduction power losses.

The traditional single-switch DC-DC boost converter with a quadratic gain formula can produce a high voltage conversion ratio at a lower duty cycle ratio. But it has the drawback of a switch voltage equal to the output voltage [21]. The theoretical and experimental validation of a non-isolated quadratic boost-based DC-DC converter with reduced structure component count, suitable for renewable energy applications, is explored in [22], where the additional features are enhanced voltage gain and continuous input current. Some authors proposed a structure of a high-gain quadratic boost converter integrated with VMC and switched capacitor circuits, optimized for electric vehicle applications [23]. The converter's performance is validated by both simulation and experimental platforms [23]. The steady-state analysis, the dynamic modeling, and the experimental results for a non-isolated ultra-high gain quadratic boost-based DC-DC converter with low switch voltage stress are presented in [24]. The research work proposed in [25] explores the closed-loop dynamic performance of a PI- and sliding-mode controller-based quadratic boost converter-three-phase inverter system fed a permanent magnet synchronous motor drive system, in which both the simulation and experimental findings are verified.

A high step-up quadratic DC-DC converter presented in [26] has certain notable merits such as improved voltage gain, decreased power switch voltage stress, high power conversion efficiency, reduced source current ripples, a common ground between input and output, and synchronized operation of power switches. Some authors proposed a non-isolated quadratic-gain DC-DC boost converter equipped with a VMC and a voltage lifter cell to achieve enhanced voltage gain [27]. The continuous conduction mode operation of the converter suggested in [27] is verified through simulation and hardware results. There are other

[1]Department of EEE, Government College of Engineering, Srirangam, Tiruchirappalli, India. E-mail: muralid@gces.edu.in
[2]Department of EEE, Sona College of Technology, Salem, India. Email: vidharshan.22eee@sonatech.ac.in

DOI: 10.59277/RRST-EE.2026.4.9

non-isolated structures of quadratic boost DC-DC converters in the literature for achieving enhanced voltage gain, reduced voltage stress on semiconductor-based components, and reduced input current ripples [28–32].

The authors in [32] suggested a quadratic gain-based non-isolated high step-up DC-DC power conversion scheme with two active power switches. The merits of the converter proposed in [32] include enhanced voltage gain, continuous input current, decreased voltage stress on semiconductor components, and high power conversion efficiency. The work suggested in this research article explores a scheme for achieving the extended voltage gain using a voltage-boosting module at the source side of the non-isolated quadratic boost converter proposed in [32]. The behavior of the quadratic boost converter proposed in this work is analyzed in steady state with relevant equivalent circuits. An experimental setup of the converter is developed to validate the theoretical performance of the converter. The advantages of the suggested converter include the relatively enhanced voltage gain compared to that of the converter in [32], reduced power switch voltage stress, and continuous source current.

The entire research work is divided into three sections. The following section illustrates the steady-state performance and operation of the suggested quadratic boost converter, along with the derivation of the voltage gain formula using the relevant inductor volt-second balance equations. The next section explores the prototype converter model implementation and its results. The final section concludes the key features of the proposed converter topology.

## 2. THE STRUCTURE AND THE OPERATING MODES OF THE SUGGESTED NON-ISOLATED QUADRATIC DC-DC BOOST CONVERTER

The steady-state continuous conduction mode behavior of the proposed non-isolated quadratic DC-DC boost converter with voltage boosting module is explained in detail in this section. The two modes of operation of the converter are discussed by means of relevant steady-state equivalent circuits and equations. The volt-second balance equations are written for the inductors to deduce the expression for the quadratic voltage gain ($G_{QC}$) of the proposed converter, as a function of the switch duty factor (k).

The suggested non-isolated form of the quadratic DC-DC boost converter is shown in Fig. 1. All the active power switches, diodes, and passive components in the converter configuration are assumed to be ideal. It consists of an input DC voltage ($V_{in}$) boosting structure comprising the interconnected module of power MOSFET switch $S_1$, inductor $L_1$, and diodes $D_1$ and $D_2$, respectively. The input DC voltage ($V_{in}$) appears in boosted form at the output of the voltage boosting module, which is used to extend the voltage gain of the quadratic boost DC-DC converter stage. The quadratic boost converter stage is energized by the output voltage of the voltage boosting structure as shown in Fig.1.

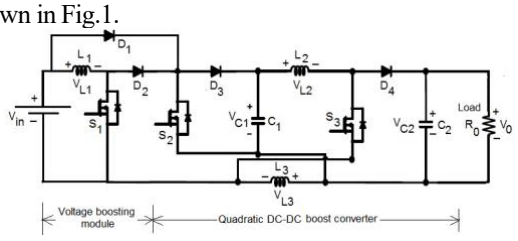



Fig. 1 – Proposed non-isolated quadratic boost DC-DC converter topology with extended voltage gain.

The quadratic boost converter section consists of two power MOSFET switches $S_2$ and $S_3$, two inductors $L_2$ and $L_3$, two diodes $D_3$ and $D_4$, and two capacitors $C_1$ and $C_2$, respectively. A load resistor $R_0$ is connected across the output of the converter. The cascaded structure of the voltage-boosting module and the quadratic DC-DC boost converter can ensure a relatively high DC output voltage ($V_0$) at a lower duty cycle ratio (k). Moreover, the voltage stress of the semiconductor-based components is relatively decreased. The two possible modes of operation of the proposed converter topology are explained in detail as illustrated below.

The equivalent structure of the converter during Mode-I operation is depicted in Fig. 2. All three power MOSFET switches $S_1$, $S_2$, and $S_3$ are simultaneously triggered into the conduction state at any switch duty factor (k) by applying the PWM (pulse-width modulated) signals with switching period $T_s$. The power switches act as a short circuit during the ON state. The diode $D_1$ is forward-biased, and hence it acts as a short-circuit path. The diodes $D_2$, $D_3$, and $D_4$ are in a reverse-biased state, and hence they act as an open-circuit path. The inductors $L_1$ and $L_3$ are charged by the source voltage $V_{in}$. Hence, the source voltage $V_{in}$ is considered as the voltage across the parallel-connected inductors $L_1$ and $L_3$ ($V_{L1} = V_{L3}$). The voltage across the inductor $L_2$ ($V_{L2}$) is the sum of the capacitor $C_1$ voltage ($V_{C1}$) and $V_{in}$. The inductor voltages are written as Eq. 1.

$$V_{L1} = V_{L3} = V_{in} \; ; \qquad V_{L2} = V_{in} + V_{C1}. \tag{1}$$

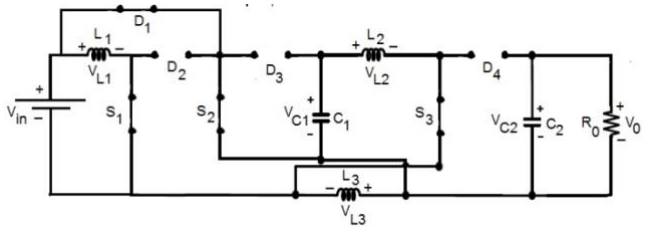


Fig. 2 – Equivalent structure during Mode-I operation of the topology.

The converter topology's Mode-II operation is illustrated by the equivalent structure shown in Fig. 3. All three power MOSFET switches $S_1$, $S_2$, and $S_3$ are now turned OFF and are represented as an open-circuited path. The diode $D_1$ is reverse-biased, and hence it is represented as an open circuit. The remaining diodes $D_2$, $D_3$, and $D_4$ start to conduct due to the forward-biased condition. The voltages across the inductors are represented as

$$V_{L1} = V_{L3} = \frac{V_{in} - V_{C1}}{2} \; ; \qquad V_{L2} = V_{C1} - V_0, \tag{2}$$

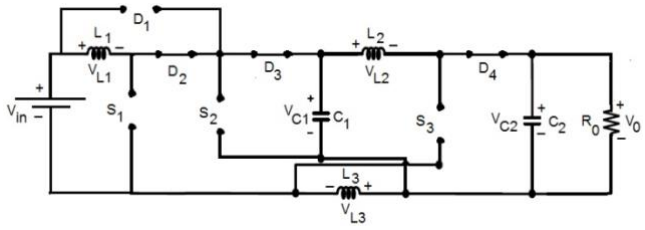


Fig. 3 – Equivalent structure during Mode-II operation of the topology.

The volt-second balance principle is applied to the inductors $L_1$, $L_2$, and $L_3$ to deduce the expression for the voltage gain of the proposed quadratic converter using eq. (1) and (2). The following volt-second balance equations are written for the three inductors.

$$V_{in} k T_s + \left(\frac{V_{in} - V_{C1}}{2}\right)(1-k)T_s = 0, \tag{3}$$

$$(V_{in} + V_{C1})kT_s + (V_{C1} - V_0)(1-k)T_s = 0. \tag{4}$$

From eq. (3), the capacitor voltage $V_{C1}$ is obtained as:

$$V_{C1} = \left(\frac{1+k}{1-k}\right) V_{in}. \quad (5)$$

The above $V_{C1}$ expression is substituted into eq. (4) to derive the expression for the voltage gain ($G_{QC}$) of the proposed quadratic converter.

$$G_{QC} = \frac{V_0}{V_{in}} = \frac{1+2k-k^2}{(1-k)^2}. \quad (6)$$

It is evident from eq. (6) that the suggested quadratic converter with a voltage-boosting module can enhance output voltage ($V_0$) levels at low duty factor (k) itself. It is also shown that the voltage gain ($G_{QC}$) of the quadratic converter suggested in this work is greatly enhanced compared with that of the other configurations of non-isolated quadratic converters in the literature, as shown in Fig. 4.

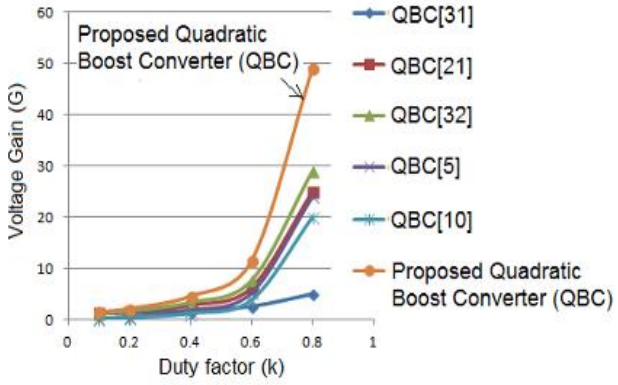



Fig. 4 – Voltage gain comparison of quadratic boost converters family.

## 3. LABORATORY MODEL OF THE PROPOSED CONVERTER AND ITS RESULTS

An experimental setup of the proposed quadratic boost-based DC-DC converter with a voltage-boosting module is built using low-power components as shown in Fig. 5, and its performance is validated at duty factor k = 0.6 for all the power MOSFET switches $S_1$, $S_2$, and $S_3$, respectively. The specifications of the converter components are given in Table 1. All the passive components are designed as per the specifications [32]. The microcontroller is employed to generate PWM signals for driving the power MOSFET switches $S_1$, $S_2$, and $S_3$, respectively, by proper modulation of the duty factor (k) of a digital output pin using internal timers/counters. In the proposed work, the dsPIC30F2010 microcontroller is used. The dsPIC30F2010 microcontroller cannot be used directly to charge the capacitance ($C_{GS}$) between the gate and source terminals of the power MOSFET switch since the microcontroller can produce low-power-level output signals only. Hence, it is required to use the TLP250H category of gate driver circuitry as an interface between the microcontroller and the MOSFET power switch. The driver circuit energized by the microcontroller's low-power output signal produces high-current PWM signals which are applied to trigger the power MOSFET switches $S_1$, $S_2$, and $S_3$ simultaneously from the non-conducting state to the conducting state. The switching pulses are shown in Fig. 6 and Fig. 7, respectively. All three MOSFET switches are switched at a frequency ($f_s$) of 30 kHz each. The proposed converter topology is energized by a battery source with a voltage rating of 12 V and a charge capacity of 7.5 Ah. The battery source voltage ($V_{in}$) and source current ($I_{in}$) waveforms of the converter are depicted in Fig. 8. An incandescent lamp load rated at 60 W is powered by the converter at a duty factor (k = 0.6), as shown in Fig. 5. Figure 9 illustrates the load voltage ($V_0$) and load current ($I_0$) waveforms. A load current of 0.430 A flows through the load at a converter output voltage of 138 V, corresponding to k = 0.6. The three inductor voltage waveforms are shown in Figs. 10 to 12, respectively. The voltage stress waveforms of all four diodes are depicted in Figs. 13 to 16, respectively. The two capacitor voltages are illustrated in Figs. 17 and 18, respectively. The voltage stresses on all three power MOSFET switches are found to be 92 V, 84 V, and 72 V, respectively, as shown in Figs. 19 to 21.

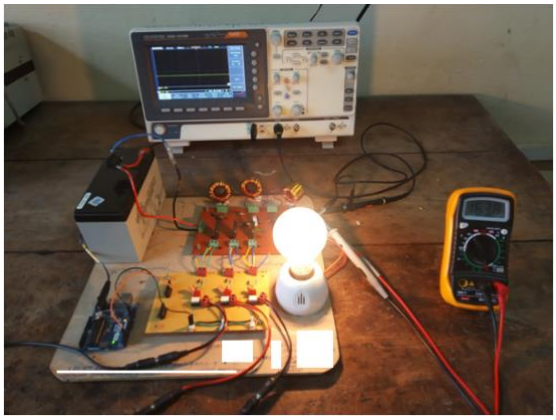


Fig. 5 – Experimental setup of the proposed converter.

*Table 1*

Specifications of converter components used in the experimental setup.

| Hardware components | Specifications |
|---|---|
| DC input source | 12 V and 7.5 Ah capacity |
| Power MOSFET switches: $S_1$, $S_2$, & $S_3$ | 2SK2645 N-Channel: 600 V, 9 A (each) |
| Diodes: $D_1$, $D_2$, $D_3$, & $D_4$ | UF5408: 1000 V, 3 A (each) |
| Microcontroller | dsPIC30F2010 |
| Driver for MOSFET | TLP250H |
| Inductors: $L_1$, $L_2$, & $L_3$ | 336 µH each |
| Capacitors: $C_1$ & $C_2$ | 33 µF, 200 V each |
| Lamp load ($R_0$) | 60 W |

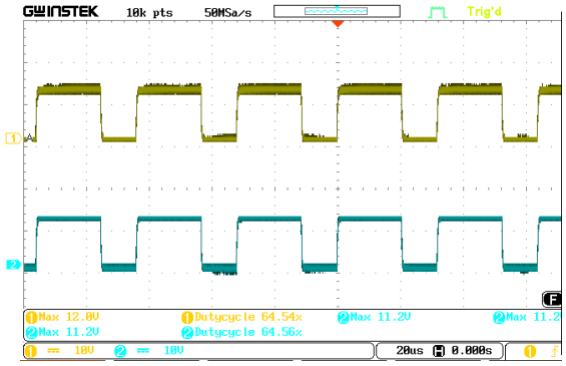



Fig. 6 – Triggering pulses applied to the switches $S_1$ and $S_2$.

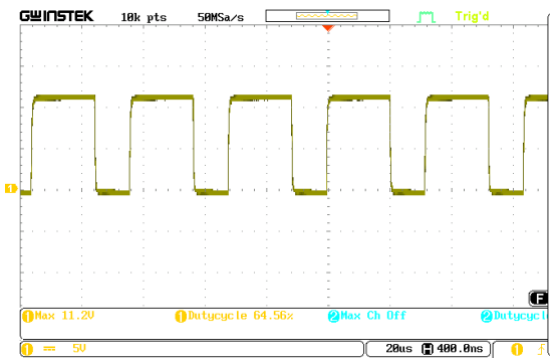



Fig. 7 – Triggering pulses applied to the switch $S_3$.

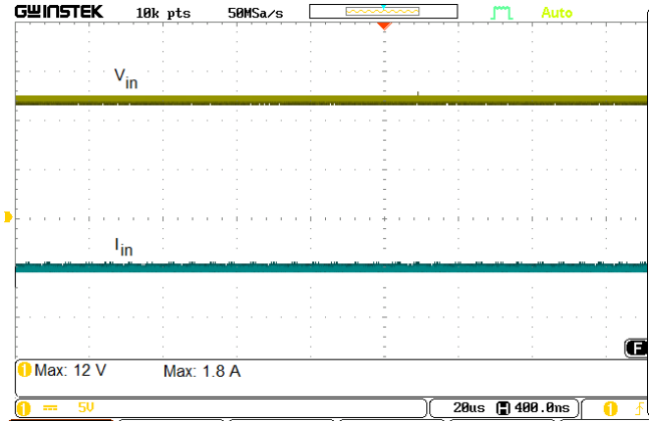



Fig. 8 – Source voltage ($V_{in}$) and source current ($I_{in}$) waveforms for the converter.

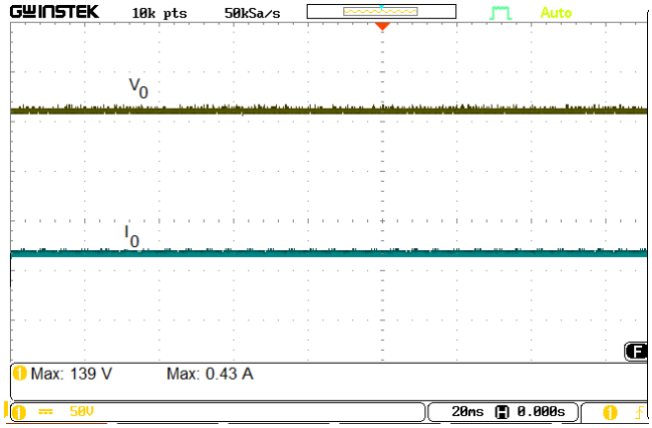



Fig. 9 – Load voltage ($V_0$) and load current ($I_0$).

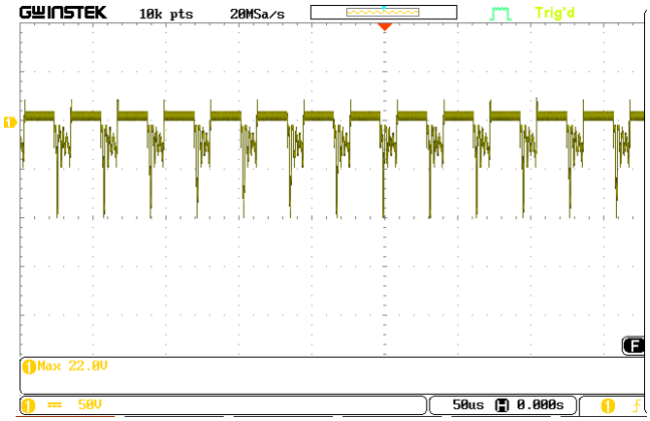



Fig. 10 – Voltage ($V_{L1}$) across the inductor $L_1$.

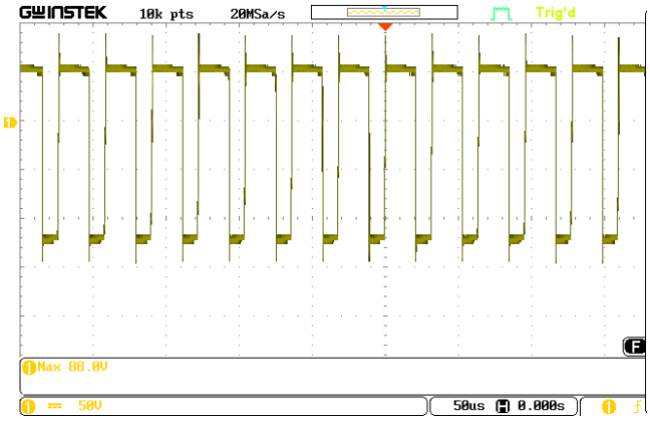



Fig. 11 – Voltage ($V_{L2}$) across the inductor $L_2$.

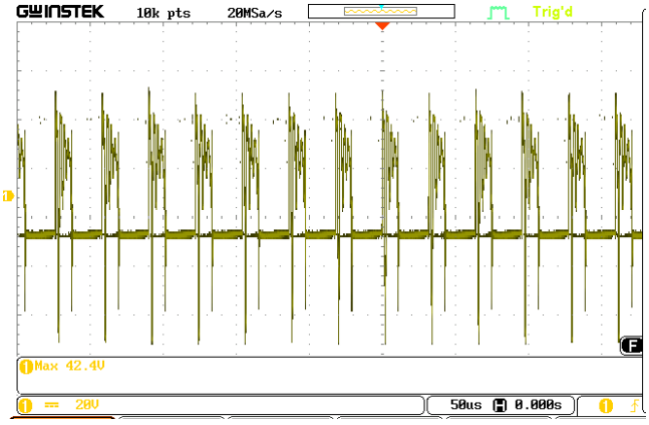



Fig. 12 – Voltage ($V_{L3}$) across the inductor $L_3$.

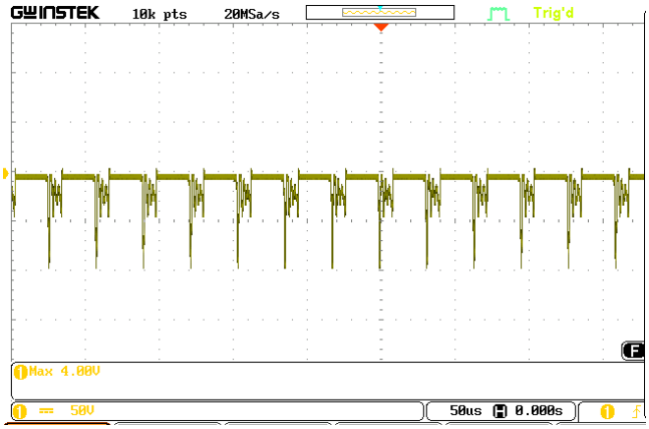



Fig. 13 – Voltage ($V_{D1}$) across the diode $D_1$.

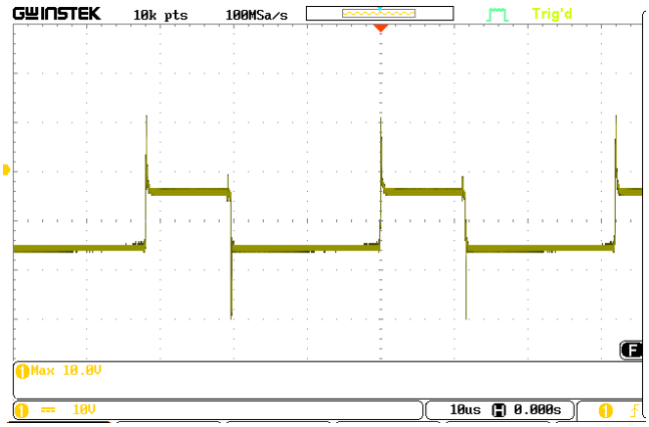



Fig. 14 – Voltage ($V_{D2}$) across the diode $D_2$

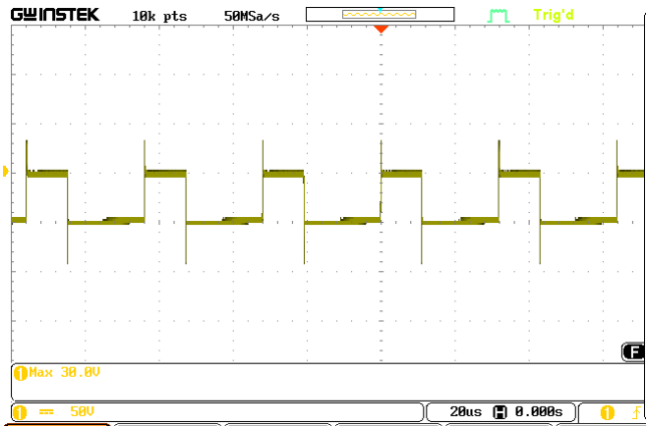



Fig. 15 – Voltage ($V_{D3}$) across the diode $D_3$.

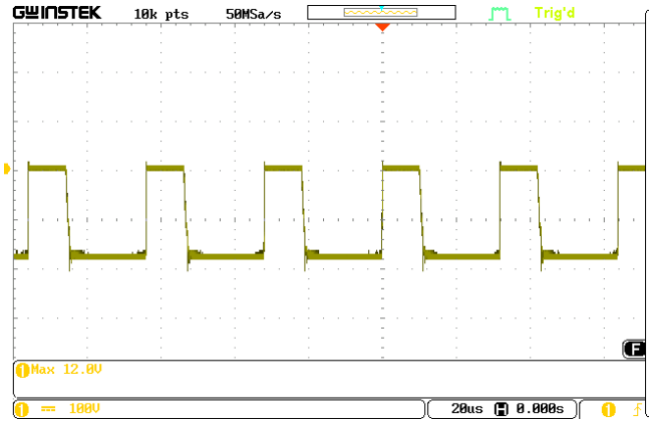



Fig. 16 – Voltage ($V_{D4}$) across the diode $D_4$.

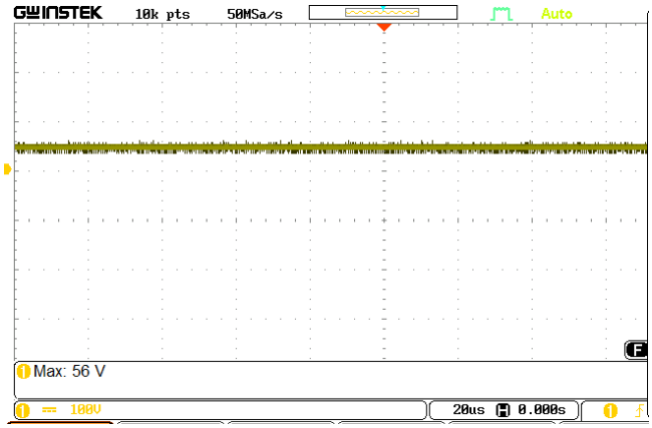



Fig. 17 – Voltage ($V_{C1}$) across the capacitor $C_1$.

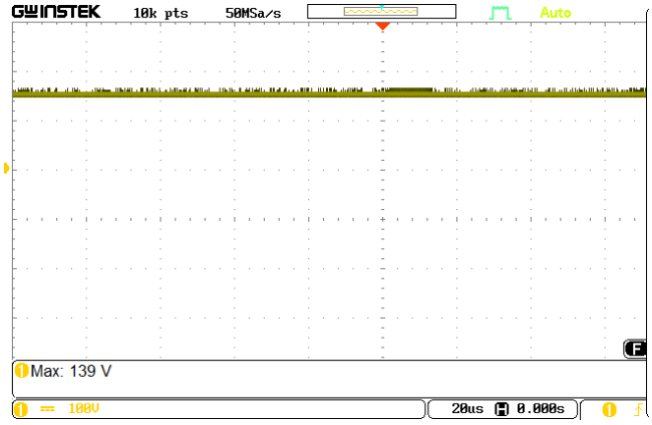



Fig. 18 – Voltage ($V_{C2}$) across the capacitor $C_2$.

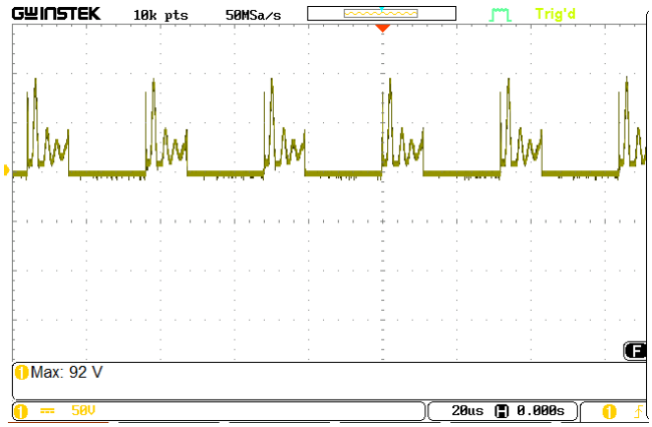



Fig. 19 – Voltage stress ($V_{S1}$) across the switch $S_1$.

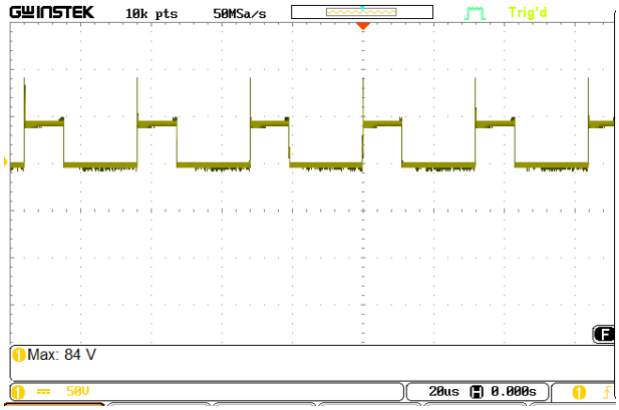



Fig. 20 – Voltage stress ($V_{S2}$) across the switch $S_2$.

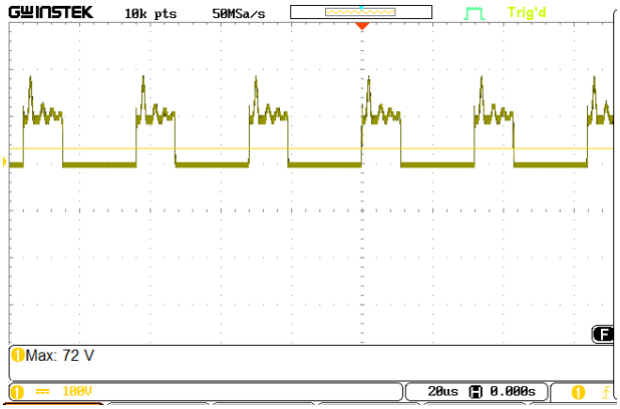



Fig. 21 – Voltage stress ($V_{S3}$) across the switch $S_3$.

## 4. CONCLUSIONS

In this research article, a non-isolated form of DC-DC converter structure with enhanced quadratic voltage gain is proposed. The extended voltage gain is achieved by incorporating a voltage-boosting module at the DC source side of the converter. The two different modes of steady-state operation of the converter are analyzed with the help of relevant converter equivalent circuits and inductor volt-second balance equations. A laboratory model of the suggested converter of 60 W rating is built with a 12 V battery source and low-power semiconductor-based as well as passive components designed as per the specifications, and its operating performance is validated through theoretical analysis. The three power MOSFET switches are simultaneously triggered into conduction mode using PWM signals at a 60% duty cycle ratio and a switching frequency ($f_s$) of 30 kHz. The features of the proposed quadratic converter include reduced component count, continuous input current, relatively enhanced quadratic voltage gain at low duty factor by means of a voltage-boosting structure, simple converter control strategy, and relatively decreased voltage stress on controlled as well as uncontrolled semiconductor devices used in the topology. The developed converter structure finds applications in renewable energy-based power generation systems, DC microgrids, and electric vehicles.

## CREDIT AUTHORSHIP CONTRIBUTION

Murali DURAISAMY: methodology; conceptualization; investigation; experimental design; writing – original draft; validation.

Vidharshan MURALI: experimental investigation; data acquisition; editing.

## ACKNOWLEDGMENT

The authors acknowledge the technical support from the Department of Electrical and Electronics Engineering, Government College of Engineering, Srirangam, Tiruchirappalli, for conducting the experimental work on the proposed converter.

*Received on 12 March 2026*

## REFERENCES

1. H.A. Mosallam, "A systematic review of DC-DC converter technologies: traditional, bidirectional, and impedance-source topologies," Discover Electronics, **3**, *16*, pp. 1–65 (2026).
2. X. Wu, J. Wang, Y. Zhang, J. Du, Z. Liu, Y. Chen, "Review of DC-DC converter topologies based on impedance network with wide input voltage range and high gain for fuel cell vehicles," Automotive Innovation, **4**, pp. 351–372 (2021).
3. P. Anbarasu, N.K. Loganathan, A. Narendran, K. Rameshkumar, "Metaheuristic-driven dual inductor boost converter for floating PV systems in MATLAB/Simulink," Rev. Roum. Sci. Techn. – Électrotechn. et Énerg., **71**, *1*, pp. 103–108 (2026).
4. N.B. Dişken, M.M. Savrun, "High-gain multi-port DC-DC converter topologies for renewable energy applications: a comprehensive review," Electric Power Components and Systems, **52**, *8*, pp. 1459–1473 (2024).
5. S.A. Gorji, A. Mostaan, H.T. My, M. Ektesabi, "Non-isolated buck-boost DC-DC converter with quadratic voltage gain ratio," IET Power Electronics, **12**, *6*, pp. 1425–1433 (2019).
6. T. Nivetha, V. Lavanya, P. Sriramalakshmi, "Review of DC-DC boost converter derived topologies for renewable energy applications," International Journal of Power Electronics and Drive Systems, **15**, *2*, pp. 947–957 (2024).
7. D. Murali, "Analysis and experimental validation of a non-isolated DC-DC SEPIC-modified CUK combined converter," Rev. Roum. Sci. Techn. – Électrotechn. et Énerg., **70**, *3*, pp. 367–372 (2025).
8. S. Coelho, V. Monteiro, J.L. Afonso, "Topological advances in isolated DC-DC converters: high-efficiency design for renewable energy integration," Sustainability, **17**, pp. 1–40 (2025).
9. Y. Supriya, J.S. Rajashekar, "A comprehensive review of various isolated DC-DC converter topologies associated with photovoltaic applications," Recent Advances in Electrical and Electronic Engineering, **15**, *8*, pp. 595–606 (2022).
10. P.K. Maroti, S. Padmanaban, J.B.H. Nielsen, M.S. Bhaskar, M. Meraj, A. Iqbal, "A new structure of high-voltage-gain SEPIC converter for renewable energy applications," IEEE Access, **7**, pp. 89857–89868 (2019).
11. G. Guerin, G.A. Rincon-Mora, "Switched-inductor DC-DC converters: direct small-signal equivalent AC circuit," Electronics, **15**, *5*, pp. 1–18 (2026).
12. P. Biswal, V.V.S.K. Bhajana, A. Iqbal, V. Kakani, M. Popuri, "Extended high gain DC-DC converter with switched-inductors, switched-capacitors and soft-switching: analysis and implementation," IET Power Electronics, **17**, *11*, pp. 1445–1456 (2024).
13. M. Kalarathi, J. Gnanavadivel, K. Jayanthi, "High-boost DC-DC converter based on switched inductor, switched capacitor and voltage multiplier cell," Iranian Journal of Science and Technology, Transactions of Electrical Engineering, **48**, pp. 965–978 (2024).
14. M.E. Azizkandi, F. Sedaghati, H. Shayeghi, F. Blaabjerg, "A high-voltage DC-DC converter based on a three-winding coupled inductor and voltage multiplier cell," IEEE Transactions on Power Electronics, **35**, *5*, pp. 4558–4567 (2020).
15. A. Alzahrani, M. Ferdowsi, P. Shamsi, "A family of scalable non-isolated interleaved DC-DC boost converters with voltage multiplier cells," IEEE Access, **7**, pp. 11707–11721 (2019).
16. D. Murali, "A transformerless boost-modified CUK combined single-switch DC-DC converter topology with enhanced voltage gain," Brazilian Archives of Biology and Technology, **66**, *3*, pp. 1–20 (2023).
17. M. Karthikeyan, R. Elavarasu, P. Ramesh, C. Bharatiraja, P. Sanjeevikumar, L. Mihet-Popa, M. Mitolo, "A hybridization of CUK and boost converter using single switch with higher voltage gain capability," Energies, **13**, *9*, pp. 1–24 (2020).
18. D. Murali, "Closed-loop implementation of a non-isolated high step-up integrated SEPIC-CUK DC-DC converter structure with single switch," Brazilian Archives of Biology and Technology, **67**, *2*, pp. 1–15 (2024).
19. K.A. Mahafzah, M.A. Obeidat, A. Mansour, E.R. Sanseverino, G. Zizzo, "A new smart grid hybrid DC-DC converter with improved voltage gain and synchronized multiple outputs," Applied Sciences, **14**, *6*, pp. 1–18 (2024).
20. S. Ranganathan, A.N.D. Mohan, "Formulation and analysis of single-switch high-gain hybrid DC-to-DC converter for high-power applications," Electronics, **10**, *19*, pp. 1–14 (2021).
21. L. Díaz-Saldierna, J. Morales-Saldaña, M. Ortiz-López, "Switching regulator using a quadratic boost converter for wide DC conversion ratios," IET Power Electronics, **2**, *5*, pp. 605–613 (2009).
22. N. Subhani, Z. May, M.K. Alam, S. Mamun, "An enhanced gain non-isolated quadratic boost DC-DC converter with continuous source current," PLoS ONE, **18**, *12*, pp. 1–25 (2023).
23. J. Gnanavadivel, M. Kalarathi, K. Prakash, "A double-switch integrated high-gain quadratic boost converter for electric vehicle applications," Rev. Roum. Sci. Techn. – Électrotechn. et Énerg., **70**, *4*, pp. 495–500 (2025).
24. A.B. Reddy, S.N. Mahato, N. Tewari, "Dual-switch ultra-high-gain DC-DC converter with low-voltage stress," International Journal of Electronics and Communication (AEU), **173**, pp. 1–11 (2024).
25. S. Bhavani, A. Sivaprakasam, "Sliding mode controlled closed-loop quadratic boost converter three-phase inverter system-fed permanent synchronous motor drive with enhanced response," Rev. Roum. Sci. Techn. – Électrotechn. et Énerg., **70**, *3*, pp. 331–336 (2025).
26. R. Rostami, S.H. Hosseini, M.B.B. Sharifian, "High-gain non-isolated step-up DC-DC converter proper for renewable energy applications," Scientific Reports, **15**, *1*, pp. 1–24 (2025).
27. S. Radhakrishnan, M. Veerasamy, "Modified multi-stage quadratic DC-DC converter with voltage multiplier for solar PV applications," International Journal of Electronics, **113**, *6*, pp. 1145-1168 (2026).
28. N. Dizangian, S. Jovanović, P. Poure, "Modeling and experimental verification of a single-switch quadratic boost DC-DC converter with high voltage gain for energy harvesting," Energies, **18**, *20*, pp. 1–31 (2025).
29. B. Babaiahgari, J.E. Valdez-Resendiz, A.A. Reyes, J.C. Rosas-Caro, E.D. Silva-Vera, "Quadratic boost converter with reduced input current ripple," Applied Sciences, **15**, *19*, pp. 1–20 (2025).
30. K. Jayanthi, S. Narthana, J. Gnanavadivel, "A single-switch non-isolated quadratic high-gain configuration for renewable energy applications," Rev. Roum. Sci. Techn. – Électrotechn. et Énerg., **71**, *1*, pp. 97–102 (2026).
31. J.L. Ramos, R.M. Varona, M.G.O. Lopez, L.H. Díaz-Saldierna, D.L. Cordoba, "Control strategy of a quadratic boost converter with voltage multiplier cell for high-voltage gain," IEEE Journal of Emerging and Selected Topics in Power Electronics, **5**, *4*, pp. 1761–1770 (2017).
32. J. Ahmad, M. Zaid, A. Sarwar, C.H. Lin, M. Asim, R.K. Yadav, M. Tariq, K. Satpathi, B. Alamri, "A new high-gain DC-DC converter with continuous input current for microgrid applications," Energies, **14**, *9*, pp. 1–14 (2021).